

# Generating highly squeezed Hybrid Laguerre–Gauss modes in large Fresnel number Degenerate Optical Parametric Oscillators

Carlos Navarrete-Benlloch, Germán J. de Valcárcel, and Eugenio Roldán  
*Departament d'Òptica, Universitat de València, Dr. Moliner 50, 46100-Burjassot, Spain*

## Abstract

We theoretically describe the quantum properties of a large Fresnel number degenerate optical parametric oscillator with spherical mirrors that is pumped by a Gaussian beam. The resonator is tuned so that the resonance frequency of a given transverse mode family coincides with the down-converted frequency. After demonstrating that only the lower orbital angular momentum (OAM) Laguerre–Gauss modes are amplified above threshold, we focus on the quantum properties of the rest of (classically empty) modes. We find that combinations of opposite OAM (Hybrid Laguerre-Gauss modes) can exhibit arbitrary large quadrature squeezing for the lower OAM non amplified modes.

PACS numbers: 42.50.Dv, 42.50.Lc, 42.50.Tx, 42.65.Yj

## I. INTRODUCTION

Degenerate optical parametric oscillators (DOPOs) are nowadays the standard squeezed light source. Let us remind that a light mode is said to be squeezed if the fluctuations in one of its quadratures are below the standard quantum limit, which is defined as the vacuum fluctuations level of that quadrature [1, 2, 3]. In DOPOs, squeezing is accomplished thanks to the parametric down-conversion process occurring in the non-linear crystal together with the interference between the intracavity field and the external vacuum fluctuations that enter into the cavity through the output mirror [4]. Quantum noise reductions as large as 10dB (90%) have been experimentally demonstrated with DOPOs [5].

High precision measurements are perhaps the best known applications of squeezed light [3], but applications to quantum information with continuous variables are becoming increasingly important [6], as squeezed light is the essential ingredient in generating continuous-variable entanglement. Improving the quality and reliability of squeezing is thus an important goal, but the generation of squeezed light with particular spatial distributions could also be important. This has been shown to be of utility in, e.g., high precision positioning [7]. Recently Laguerre–Gauss beams are attracting much attention because of the many potential applications of the orbital angular momentum (OAM) carried by these light beams [8], and the generation of non classical Laguerre–Gauss modes could thus lead to new phenomena in the interaction between these light fields and matter.

Here we consider squeezing generation by means of DOPOs with large Fresnel number cavities with spherical mirrors. In such systems, the cavity can sustain the non-linear interaction for many transverse modes (diffraction losses are ideally suppressed) giving rise to new results concerning squeezing. Quantum fluctuations in large Fresnel number cavities have been studied in the past, and new phenomena resulting from the interplay between quantum fluctuations and transverse pattern formation have been predicted. Concerning plane cavity mirrors, the phenomena of quantum images [9] (below thresh-

old) and the perfect non-critical squeezing of the emerging transverse pattern linear momentum [10, 11] (above threshold) have been predicted. Regarding spherical mirrors, only below threshold operation has been studied [12], showing that also in this case there appear quantum images anticipating the above threshold pattern.

Here we consider a DOPO cavity with spherical mirrors that is pumped by a Gaussian mode. We shall assume that the cavity is exactly tuned to a particular family of Laguerre–Gauss transverse modes (a family  $f$  consists of  $f + 1$  Laguerre–Gauss modes with OAM  $\pm f, \pm(f-2), \dots, \pm l_0$  with  $l_0 = 0$  or 1 for even or odd  $f$  respectively, this is reviewed in Section II below). After deriving in Section III the system's model, we first demonstrate (Section IV) that the DOPO will emit, above threshold, a signal field consisting of pairs of photons with OAM  $+l_0$  and  $-l_0$ , i.e., the DOPO emits in the transverse mode with the lower possible OAM. The squeezing properties of this mode coincide with those derived in the past, as the case  $l_0 = 0$  is equivalent to the standard DOPO model [2], and the case  $l_0 = 1$  generalizes what has recently been described in [13]. After reviewing the squeezing properties of cases  $l = 0$  and 1 in Subsection V.A, we concentrate in the squeezing properties of the rest of modes (those with  $l > l_0$  that remain off when the DOPO is above threshold) in Subsection V.B. We will demonstrate that certain combinations of opposite OAM modes exhibit large squeezing (which is larger for the larger values of  $f$  and the lower values of  $l$ ). This squeezing is non-critical, i.e., is independent of the pumping value. This result, that admits a simple explanation (Subsection V.C), is a main result of this work and we find it relevant because it establishes a simple way for generating squeezed vacua with shapes different from the Gaussian or TEM<sub>10</sub> ones. In Section VI we review the main conclusions of our work.

## II. CAVITY MODES

For the sake of clarity, we find it most convenient to review the main properties of the cavity modes in a Fabry-

Perot resonator with spherical mirrors (see, e.g., [14] for more details). Within the paraxial approximation, it is well known that the Laguerre-Gauss modes form a complete set of spatial modes describing the light inside the resonator. Let  $R_1$  and  $R_2$  denote the curvature radius of the cavity mirrors, and  $L_{eff} = L - (1 - 1/n_c)l_c$  the effective cavity length, being  $L$  the geometrical length of the resonator, and  $l_c$  and  $n_c$  the length and refractive index, respectively, of the  $\chi^{(2)}$  crystal. Then the Laguerre-Gauss modes at the resonator waist plane can be written as

$$\Psi_p^{\pm l}(\mathbf{r}) = \mathcal{N}_p^l u_p^l(r) \exp[\pm il\phi], \quad (1)$$

with  $\mathbf{r} = (x, y)$  the transverse coordinates being  $\mathbf{r} = r(\cos\phi, \sin\phi)$  its polar decomposition,  $\mathcal{N}_p^l$  a normalization factor and

$$u_p^l(r) = \frac{1}{w} \left( \frac{\sqrt{2}r}{w} \right)^l L_p^l \left( \frac{2r^2}{w^2} \right) \exp \left[ -\frac{r^2}{w^2} \right], \quad (2)$$

being  $L_p^l$  the modified Laguerre polynomial with radial and polar indices  $p, l \in \mathbb{N}$ , which are given by Rodrigues formula

$$L_p^l(v) = \frac{1}{p!} e^v \frac{1}{v^l} \frac{d^p}{dv^p} (e^{-v} v^l v^p). \quad (3)$$

By choosing the normalization factor as

$$\mathcal{N}_p^l = \sqrt{\frac{2}{\pi} \frac{p!}{(p+l)!}}, \quad (4)$$

the following orthogonality relation holds

$$\int_0^{2\pi} d\phi \int_0^\infty r dr [\Psi_p^{\pm l}(\mathbf{r})]^* \Psi_{p'}^{\pm l'}(\mathbf{r}) = \delta_{ll'} \delta_{pp'}. \quad (5)$$

The beam spot size at the cavity waist,  $w$ , is given by

$$w^2 = \frac{2cL_{eff}}{\omega} \frac{\sqrt{g_1 g_2 (1 - g_1 g_2)}}{g_1 + g_2 - 2g_1 g_2}, \quad (6)$$

with  $g_j = 1 - L_{eff}/R_j$  and  $\omega$  the beam frequency.

The Laguerre-Gauss basis is recommended in order to visualize the OAM of the field, as these modes are eigenstates of the OAM operator  $-i\partial_\phi$  with eigenvalues  $\pm l$ . Concerning the resonance frequency of the different  $\Psi_p^{\pm l}$  modes, they are different in general for each mode. Concretely  $\omega_{qpl} = q\pi c/L_{eff} + \Delta\omega_{pl}$ , with  $q$  an integer (different  $q$ 's correspond to different *longitudinal* cavity modes) and the *transverse* part of the resonance frequency is given by

$$\Delta\omega_{pl} = \frac{c}{L_{eff}} (1 + 2p + l) \cos^{-1}(\sqrt{g_1 g_2}). \quad (7)$$

Hence, cavity modes having the same *family order*  $f = (2p + l)$  have the same frequency and are said to be members of the same family  $f$ . It is clear that family  $f$  consists of the set of  $f+1$  Laguerre-Gauss modes  $\{\Psi_{(f-l)/2}^{\pm l}\}$ ,

with  $l = f, f-2, \dots, l_0$ , having OAM  $\pm f, \pm(f-2), \dots, \pm l_0$ , respectively. The lower OAM modes have  $l_0 = 0$  or 1 for even or odd  $f$  respectively. In Fig. 1 we represent  $\omega_{qpl}$  (in units of the *free spectral range*,  $f_{sr} = \pi c/L_{eff}$ ) for several modes as a function of  $g$  for *symmetric* resonators (those for which  $g_1 = g_2 \equiv g$ ) which are *stable* (i.e.,  $-1 < g < 1$ ; remind that  $g = 1$  corresponds to plane mirrors,  $g = 0$  to a confocal resonator, and  $g = -1$  to a concentric resonator). It can be clearly appreciated that different transverse families corresponding to different longitudinal modes can have the same frequency for rational values of  $(\cos^{-1} g)/\pi$ . Below we assume that the families have different frequencies, i.e., that this quantity has an irrational value.

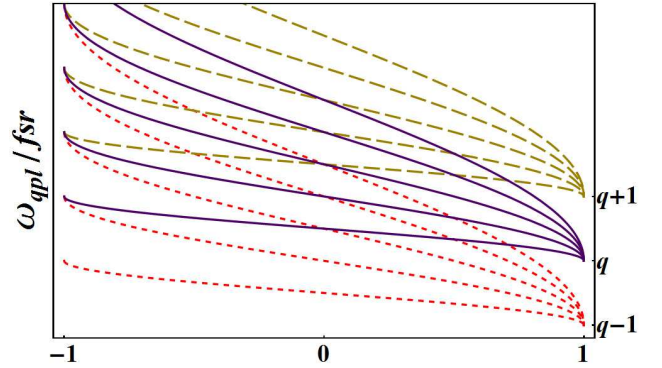


Fig. 1.- Resonance frequencies of the first 4 families corresponding to 3 consecutive longitudinal modes, as a function of the  $g$  parameter of a symmetrical resonator. Different families corresponding to the same longitudinal mode have the same color and dashed. The family order  $f$  increases with the frequency.

Before going on we recall that another basis can be formed from the Laguerre-Gauss basis, which is usually referred to as *Hybrid Laguerre-Gauss* basis (*Hybrid* basis for short). It is obtained by the sum and the difference of Laguerre-Gauss modes with opposite OAM and its analytic expression at the waist plane of a Fabry-Perot resonator reads

$$H_{j,p}^l(\mathbf{r}) = \sqrt{2} \mathcal{N}_p^l \cdot u_p^l(r) \cdot \begin{cases} \cos l\phi & \text{for } j = c \\ \sin l\phi & \text{for } j = s \end{cases} \quad (8)$$

In this expression  $l \neq 0$  since  $H_p^0 = \Psi_p^0$ . We will see later that these are the most appropriate modes in order to understand the squeezing properties of our system, although the Laguerre-Gauss basis is more appropriate for carrying out the necessary calculations.

### III. DOPO'S QUANTUM MODEL

Consider that the optical cavity is pumped by a coherent Gaussian pump of frequency  $2\omega_0$  that is matched to the fundamental transverse mode  $\Psi_0^0$ . Within the cavity,

pump photons are down-converted into signal photons of frequency  $\omega_0$  at a  $\chi^{(2)}$  crystal that is placed at the cavity waist. The important assumption of this work is that the resonator is tuned so that  $\omega_0$  coincides with the resonance frequency of a single transverse family  $f$ , and is detuned far enough from any other family. Within these conditions, the field at the resonator waist plane can be written as

$$\hat{E}(\mathbf{r}, t) = \hat{E}_p(\mathbf{r}, t) + \hat{E}_s(\mathbf{r}, t), \quad (9a)$$

$$\hat{E}_p(\mathbf{r}, t) = i\mathcal{F}_p \hat{A}_p(\mathbf{r}, t) e^{-2i\omega_0 t} + H.c., \quad (9b)$$

$$\hat{E}_s(\mathbf{r}, t) = i\mathcal{F}_s \hat{A}_s(\mathbf{r}, t) e^{-i\omega_0 t} + H.c., \quad (9c)$$

with slowly varying envelopes

$$\hat{A}_p(\mathbf{r}, t) = \hat{a}_{00}(t) \Psi_0^0(\mathbf{r}), \quad (10a)$$

$$\hat{A}_s(\mathbf{r}, t) = \sum_l \frac{1}{(1 + \delta_{0l})} \left[ \hat{a}_{+l}(t) \Psi_{(f-l)/2}^{+l}(\mathbf{r}) + \hat{a}_{-l}(t) \Psi_{(f-l)/2}^{-l}(\mathbf{r}) \right], \quad (10b)$$

with  $\delta_{0l}$  is the Kronecker symbol. The sum in  $l$  is understood to be extended to all the members of the set  $\{f, f-2, \dots, l_0\}$  and this will hold for all sums in  $l$  along the rest of the article. We have introduced the *single-photon field voltages*

$$\mathcal{F}_p = \sqrt{2} \mathcal{F}_s = \sqrt{\frac{2\hbar\omega_0}{\varepsilon_0 n_c L_{eff}}}, \quad (11)$$

and the boson operators for modes  $m$  and  $n$  obey the canonical commutation relations  $[\hat{a}_m, \hat{a}_n^\dagger] = \delta_{mn}$ . Finally, note that the Laguerre-Gauss modes appearing in (10a) and (10b) are evaluated at pump and signal frequency respectively.

For the sake of later use we mention here that instead of the Laguerre-Gauss modes, one can use the Hybrid modes in order to expand the slowly varying envelope of the signal field. This expansion would allow us to define annihilation and creation operators for these modes, which are easily found to be related to the Laguerre-Gauss operators by

$$\hat{a}_{c,l} = [\hat{a}_{+l}(t) + \hat{a}_{-l}(t)] / \sqrt{2}, \quad (12a)$$

$$\hat{a}_{s,l} = i [\hat{a}_{+l}(t) - \hat{a}_{-l}(t)] / \sqrt{2}, \quad (12b)$$

where the operator  $\hat{a}_{j,l}$  is the annihilation operator related to the hybrid mode  $H_{j,p}^l$ . As before, these relations are not valid for  $l = 0$  where the boson operators for Hybrid and Laguerre-Gauss modes are exactly the same.

In the interaction picture, assuming perfect phase-matching as well as exact resonance between the fields' frequencies and the cavity resonances, the Hamiltonian of the system is  $\hat{H} = \hat{H}_{ext} + \hat{H}_{int}$ , with

$$\hat{H}_{ext} = i\hbar \mathcal{E}_p (\hat{a}_{00}^\dagger - \hat{a}_{00}), \quad (13a)$$

$$\hat{H}_{int} = i\hbar \sum_l \frac{\chi_l}{1 + \delta_{0l}} (\hat{a}_{00} \hat{a}_{+l}^\dagger \hat{a}_{-l}^\dagger - \hat{a}_{00}^\dagger \hat{a}_{+l} \hat{a}_{-l}), \quad (13b)$$

where  $\hat{H}_{ext}$  describes the external pumping process and  $\hat{H}_{int}$  describes the down-conversion process occurring in the  $\chi^{(2)}$  crystal. Notice that OAM conservation imposes the creation/annihilation of a pair of photons each with an opposite value of  $l$ .

The nonlinear coupling constants  $\chi_l$  in  $\hat{H}_{int}$  read

$$\chi_l = 12 \frac{\chi^{(2)} l_c}{w_p} \left( \frac{\omega_0}{n_c L_{eff}} \right)^{3/2} \sqrt{\frac{\hbar}{\pi \varepsilon_0}} I_l \quad (14)$$

with  $\chi^{(2)}$  the second order susceptibility of the nonlinear crystal,  $w_p$  the beam spot size at the pump frequency and

$$I_l = \frac{[(f-l)/2]!}{[(f+l)/2]!} \int_0^{+\infty} du e^{-2u} u^l \left[ L_{(f-l)/2}^l(u) \right]^2,$$

and are proportional to the overlapping integrals between the three modes involved in the particular parametric process. This means that the nonlinear coupling between pump and signal photons is larger the lower is the OAM of the latter ones, i.e.,  $\chi_f < \chi_{f-2} < \dots < \chi_{l_0}$ . This property will play an important role as we show below. Let us finally remark the the pump parameter  $\mathcal{E}_p$  is proportional to the external pump amplitude and is taken as real without loss of generality.

We will be interested in calculating normally ordered correlations of different modes, and to do so we use the generalized  $P$ -representation and its equivalent set of Langevin equations [16]. In this representation to every pair of boson operators  $(\hat{a}_j, \hat{a}_j^\dagger)$  it corresponds a pair of independent stochastic amplitudes  $(\alpha_j, \alpha_j^+)$  which are complex-conjugated in average, i.e.,  $\langle \alpha_j^+ \rangle = \langle \alpha_j \rangle^*$ . The equations of evolution of these amplitudes are derived by following the standard procedure [17, 18], see Appendix I. Assuming that losses occur just in one of the cavity mirrors at rates  $\gamma_p$  for the pump mode and  $\gamma_s$  for all possible transverse signal modes (hence the assumption of a large Fresnel number resonator) the Langevin equations of the system read

$$\dot{\alpha}_{00} = \mathcal{E}_p - \gamma_p \alpha_{00} - \sum_l \frac{\chi_l}{1 + \delta_{0l}} \alpha_{+l} \alpha_{-l}, \quad (15a)$$

$$\dot{\alpha}_{00}^+ = \mathcal{E}_p - \gamma_p \alpha_{00}^+ - \sum_l \frac{\chi_l}{1 + \delta_{0l}} \alpha_{+l}^+ \alpha_{-l}^+, \quad (15b)$$

$$\dot{\alpha}_{\pm l} = -\gamma_s \alpha_{\pm l} + \chi_l \alpha_{\mp l}^+ \alpha_{00} + \sqrt{\chi_l \alpha_{00}} \xi_{\pm l}(t), \quad (15c)$$

$$\dot{\alpha}_{\pm l}^+ = -\gamma_s \alpha_{\pm l}^+ + \chi_l \alpha_{\mp l} \alpha_{00}^+ + \sqrt{\chi_l \alpha_{00}^+} \xi_{\pm l}^+(t), \quad (15d)$$

where  $\xi_{-l}(t) = \xi_l^*(t)$  and  $\xi_{-l}^+(t) = [\xi_l^+(t)]^*$ . The noises  $(\xi_l, \xi_l^+)$  are independent complex noise sources verifying  $\langle \xi_l(t) \rangle = \langle \xi_l^+(t) \rangle = 0$  and

$$\langle \xi_l(t) \xi_{l'}^*(t') \rangle = \langle \xi_l^+(t) [\xi_{l'}^+(t')]^* \rangle = \delta_{ll'} \delta(t - t'), \quad (16)$$

being null the rest of correlations.

Within the generalized  $P$ -representation, we define the amplitude and phase quadratures, respectively, of a mode  $j$  as  $X_j = (\alpha_j^+ + \alpha_j)$  and  $Y_j = i(\alpha_j^+ - \alpha_j)$ . Outside the cavity, it is measured the variance spectrum of quadrature  $X_j$  (analogously for  $Y_j$ ), which can be calculated as  $V_{x,j}^{out}(\omega) = 1 + S_{x,j}^{out}(\omega)$ , with the squeezing spectrum given, as a function of the intracavity amplitudes, by [4]

$$S_{x,j}^{out}(\omega) = 2\gamma_j \int_{-\infty}^{+\infty} d\tau e^{-i\omega\tau} \langle X_j(t), X_j(t+\tau) \rangle, \quad (17)$$

where the factor  $2\gamma_j$  comes from the input-output relations [19]. We use the notation  $\langle a, b \rangle = \langle ab \rangle - \langle a \rangle \langle b \rangle$ . Notice that  $S_{x,j}^{out}(\omega_s) = -1$  signals perfect squeezing outside the cavity for quadrature  $\hat{X}_j$  at detection frequency  $\omega_s$  (which must not be confused with the optical frequency, as it has contributions of every pair of modes lying in opposite sidebands around the optical frequency  $\omega_j + \omega_s$ , where  $\omega_j$  is the carrier frequency of the detected mode [4]). Hence, by solving the Langevin equations for the amplitudes  $\alpha_j$  in terms of the noises  $\xi_k$ , one is able to obtain the variances of the quadratures involved in the problem, and thus the squeezing properties of the field.

#### IV. CLASSICAL EMISSION

The classical equations describing the field inside the DOPO are obtained from the quantum Langevin ones by identifying the stochastic amplitudes  $\alpha_j$  with the classical normal variables of each mode, by making  $\alpha_j^+ \rightarrow \alpha_j^*$ , and by neglecting noise terms. They read

$$\dot{\alpha}_{00} = \mathcal{E}_p - \gamma_p \alpha_{00} - \sum_l \frac{\chi_l}{1 + \delta_{0l}} \alpha_{+l} \alpha_{-l}, \quad (18a)$$

$$\dot{\alpha}_{\pm l} = -\gamma_s \alpha_{\pm l} + \chi_l \alpha_{\mp l}^* \alpha_{00}. \quad (18b)$$

Eqs. (18) have two types of stationary solutions. If we define the normalized pump parameter as

$$\sigma = \frac{\chi_{l_0}}{\gamma_p \gamma_s} \mathcal{E}_p, \quad (19)$$

it is easy to prove that the below-threshold solution

$$\bar{\alpha}_{00} = \mathcal{E}_p / \gamma_p, \quad \bar{\alpha}_l = 0 \quad \forall l, \quad (20)$$

is stable for  $\sigma < 1$  and unstable for  $\sigma > 1$  ( $\sigma = 1$  thus defines the classical threshold for emission). Apart from this *trivial* solution, there are  $(f - l_0)/2 + 1$  possible stationary solutions in which the signal field is non-zero. The form of these solutions is

$$\bar{\alpha}_{00} = \gamma_s / \chi_k, \quad \bar{\alpha}_{\pm l} = 0 \quad \forall l \neq k, \quad (21a)$$

$$\bar{\alpha}_{\pm k} = \rho_k e^{\mp i\theta_k}, \quad \rho_k^2 \equiv \frac{1 + \delta_{0k}}{g^2 \kappa_k} \left( \sigma - \frac{1}{\kappa_k} \right), \quad (21b)$$

with

$$g = \frac{\chi_{l_0}}{\sqrt{\gamma_p \gamma_s}}, \quad \text{and} \quad \kappa_k = \frac{\chi_k}{\chi_{l_0}}. \quad (22)$$

As for the phases  $\theta_k$ ,  $\theta_0 = 0$  and  $\theta_{k \neq 0} = \theta$  is arbitrary. The arbitrariness of phase  $\theta$  appears because Eqs. (18) have the symmetry  $\alpha_{\pm l} \rightarrow \alpha_{\pm l} \exp(\pm i\beta)$ , reflecting the rotational invariance of the system, which leaves undefined the phase difference between opposite OAM modes.

As for the stability, it is easy to show that the only solution that is linearly stable above threshold is precisely that in which the lower OAM modes are switched on, i.e., Eq. (21) for  $k = l_0$ . These are, in fact, the solutions with the lowest threshold  $\sigma = 1$ , see Eq. (21), as  $\chi_{l_0} > \chi_l$  as already stressed, see Eq. (14). These solutions read, in the hybrid basis, as

$$\bar{A}_s(\mathbf{r}) = \rho_0 H_{f/2}^0(r) \quad \text{for even } f \quad (23a)$$

$$\bar{A}_s(\mathbf{r}) = \sqrt{2} \rho_1 H_{c,(f-1)/2}^1(r, \phi - \theta) \quad \text{for odd } f \quad (23b)$$

with  $\rho_j$  given by Eq. (21). In Fig. 2 the square modulus of these slowly varying envelopes are shown for the first four families. Notice that the rotational symmetry of the system is broken only for odd families.

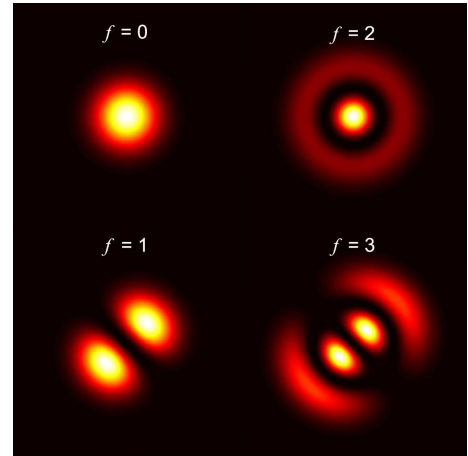


Fig. 2.- Transverse profile of the signal field modulus above threshold.

#### V. SQUEEZING

Now we undertake the analysis of quantum fluctuations in our DOPO model. First, in order to make the calculations as simple as possible, we consider the limit  $\gamma_p \gg \gamma_s$  in which the pump mode can be adiabatically eliminated in Eqs. (15). The resulting equations read

$$\dot{\alpha}_{\pm l} = -\gamma_s (\alpha_{\pm l} - n_l \alpha_{\mp l}^+) + \sqrt{\gamma_s n_l} \xi_{\pm l}(t), \quad (24a)$$

$$\dot{\alpha}_{\pm l}^+ = -\gamma_s (\alpha_{\pm l}^+ - n_l^+ \alpha_{\mp l}^+) + \sqrt{\gamma_s n_l^+} \xi_{\pm l}^+(t), \quad (24b)$$

where

$$n_l = \kappa_l \left( \sigma - g^2 \sum_{l'} \frac{\kappa_{l'}}{1 + \delta_{0l'}} \alpha_{+l'} \alpha_{-l'} \right),$$

and  $n_l^+$  is as  $n_l$  but replacing  $\alpha_j$  by  $\alpha_j^+$  in their expressions.

Next we split amplitudes  $\alpha_j$  into their classical part and that excited by quantum fluctuations, see (21),

$$\alpha_{\pm l_0}(t) = [\rho_{l_0} + b_{\pm l_0}(t)] e^{\mp i \theta_{l_0}(t)}, \quad (26a)$$

$$\alpha_{\pm l}(t) = b_{\pm l}(t). \quad (26b)$$

(for  $\alpha_j^+$  as above, but replacing  $b_j$  by  $b_j^+$  and changing the sign of  $\theta_{l_0}$ ). We have taken the phase  $\theta_{l_0}$  as an explicit variable in our quantum analysis. This is because we want to track this phase, which is undefined in the classical solution, Eq. (21), as its physical meaning is the orientation of the classical structure which breaks the system's rotational symmetry [13]. Notice also that for  $l \neq l_0$  the amplitudes are due solely to quantum fluctuations, as the classical solution for these modes is just zero.

The last assumption we make in the following is that we are working in the limit where the classical emission dominates over quantum fluctuations, i.e.,  $\rho_{l_0} \gg b_j$ , the so-called large photon number limit. In this situation we can treat  $b_j$ ,  $\xi_j$  and  $\dot{\theta}$  as small quantities and linearize the Langevin equations with respect to them. As we show below, in this limit the evolution of the different  $l$  pairs is decoupled, what allows us to analyze separately the quantum properties of each  $l$  couple. We are going to distinguish between the special cases  $l = 0$  and  $l = 1$ , on the one hand, whose squeezing properties are equivalent to that of other systems which have been analyzed in the past and we review briefly below, and cases with  $l \neq l_0$  which are analyzed here for the first time.

#### A. Special cases $l = l_0$ : Review of previously known results

The lower OAM modes of our model mimic the behaviour of both the standard single-mode DOPO [2] (for even families) and the two-transverse modes model we treated in [13] (for odd families). This is clearly apparent as OAM conservation forces the combination of a  $+l$  photon with a  $-l$  one, and hence modes with different value of  $l$  are not coupled among them in the linearized approach we use. This implies that the fluctuation properties of our model contain, in particular, those described in previous works. Let us first briefly review these known results before presenting new results in the following subsection.

As stated, for even  $f$  the only stationary solution which is stable above threshold is that corresponding to a Gaussian-like beam, i.e., a single rotationally symmetric mode with  $l = l_0 = 0$ . If modes with  $l > 0$  are ignored in (24), the equations of evolution for this mode  $l = 0$  are exactly those of the standard DOPO model, which has been analyzed many times and is by now well known (see, e.g., [2]). Here we only need to mention that perfect squeezing, in the linear approximation we adopt here, occurs only at threshold, i.e., at  $\sigma = 1$ , the squeezing level

degrading as the system is brought apart from this critical point. That is why we speak about *critical squeezing* in this case, as the system parameters need to be tuned to a particular value for obtaining the optimum squeezing level. This is a consequence of the existence, at the bifurcation point, of a null eigenvalue and of a companion negative eigenvalue with its minimum possible value. The former is the responsible for the "infinite" fluctuations of the amplitude quadrature of the signal mode (which is proportional to the eigenvector associated to the null eigenvalue), while the latter is the responsible of the complete suppression (in the linear approximation, let us insist) of the fluctuations in the signal mode phase quadrature.

Case  $l = l_0 = 1$ , in which the signal field consists of pairs of photons with opposite value of the OAM, has been studied by us very recently for the first time [13] in the case of the first transverse family ( $f = 1$ ). In this case there are two signal modes (those with OAM  $+1$  and  $-1$ ) whose stability is governed by four eigenvalues. Two of them behave like in the case  $l = 0$  above (i.e., this system also exhibits the critical squeezing at the bifurcation that we have commented above [13]). The two other eigenvalues behave very differently and are the responsible of the remarkable squeezing properties of this system: Above threshold one of them is always zero (the eigenvector associated to this eigenvalue is said to be a Goldstone mode), reflecting the indeterminacy of the phase difference between the two signal modes, see Eq. (21). This phase difference is nothing but the orientation of the bright TEM<sub>10</sub> mode that results from the coherent superposition of the  $\Psi_0^{+1}$  and  $\Psi_0^{-1}$  modes. Thus the physical meaning of the Goldstone mode is that the orientation of the signal TEM<sub>10</sub> emitted above threshold by this DOPO diffuses with time, and is thus undetermined. As for the fourth eigenvalue, it always takes its minimum possible value and its associated eigenvector has no fluctuations at all. This last eigenvector can be easily identified with the OAM of the emitted pattern, which, again, is a TEM<sub>10</sub> mode but crossed (orthogonal) with respect to the bright one. In resume: Above threshold, this DOPO emits a bright field with the shape of a TEM<sub>10</sub> whose orientation diffuses with time, and emits a perfectly squeezed vacuum again with the shape of a TEM<sub>10</sub> mode but rotated  $\pi/2$  with respect to the bright one. Remarkably this is *non-critical squeezing* because the Goldstone mode is always there if the system is above threshold. Moreover, the diffusion of the emitted field mode orientation (and, consequently, of the emitted squeezed vacuum orientation) is fortunately very slow when the system is reasonably well above threshold, what is essential for the detectability of the phenomenon.

Equations (24) particularized for  $l = 1$  coincide with the model equations of reference [13] once the  $l > 1$  modes are neglected within the linear approximation. Hence, all the properties explained above hold for the lower OAM modes of other odd families, just changing the TEM<sub>10</sub> modes for the corresponding Hybrid modes

$H_{j,(f-1)/2}^1$ . This shows that the generation of non critical squeezing through the spontaneous rotational symmetry breaking mechanism is not particular of the model considered in [13], but should be a general phenomenon. We address the reader to [13] for full details of this phenomenon, though the final result can be found below, see Eq. (36) and the subsequent comment.

### B. Special cases $l > l_0$ : Squeezing of higher OAM modes

We have shown that the system will emit in either a  $l = 0$  or a  $l = 1$  Hybrid mode, depending on the tuning selection ( $f$  even or odd, respectively). The rest of modes, those with larger OAM ( $l > l_0$ ), remain off even when the system is above threshold. We analyze now their squeezing properties.

Having tuned the cavity to family  $f$  leaves us with  $(f - l_0)/2$  pairs of modes with  $l > l_0$ . By substituting (26) into Eqs. (24) and linearizing (remind that  $b_j$ ,  $\xi_j$  and  $\theta$  are treated as small quantities), the equations ruling the evolution of the empty modes read

$$\dot{\mathbf{b}}_l = \mathcal{L}_l \mathbf{b}_l + \sqrt{\kappa_l \gamma_s} \boldsymbol{\xi}_l(t), \quad (27)$$

with

$$\mathbf{b}_l = \text{col}(b_{+l}, b_{+l}^+, b_{-l}, b_{-l}^+), \quad (28a)$$

$$\boldsymbol{\xi}_l = \text{col}(\xi_l(t), \xi_l^+(t), \xi_l^*(t), [\xi_l^+(t)]^*), \quad (28b)$$

$$\mathcal{L}_l = -\gamma_s \begin{pmatrix} 1 & 0 & 0 & -\kappa_l \\ 0 & 1 & -\kappa_l & 0 \\ 0 & -\kappa_l & 1 & 0 \\ -\kappa_l & 0 & 0 & 1 \end{pmatrix}, \quad (28c)$$

where we stress that  $0 < \kappa_l < 1$  (see Eqs. (22)).

Linear matrix  $\mathcal{L}_l$  has eigenvalues  $\lambda_1^l = \lambda_2^l = -\gamma_s(1 - \kappa_l)$  and  $\lambda_3^l = \lambda_4^l = -\gamma_s(1 + \kappa_l)$  with corresponding eigenvectors [15]

$$\mathbf{w}_{1,2}^l = \frac{1}{2} \text{col}(1, \pm 1, \pm 1, 1), \quad (29a)$$

$$\mathbf{w}_{3,4}^l = \frac{1}{2} \text{col}(1, \pm 1, \mp 1, -1). \quad (29b)$$

By projecting the linear Langevin system (27) onto  $\mathbf{w}_j^l$ , we find four equations for the projections  $c_j^l = \mathbf{w}_j^l \cdot \mathbf{b}_l(t)$

$$\dot{c}_{1,4}^l = -\gamma_s(1 \mp \kappa_l) c_1^l + \sqrt{\kappa_l \gamma_s} \eta_{1,4}^l, \quad (30a)$$

$$\dot{c}_{2,3}^l = -\gamma_s(1 \mp \kappa_l) c_3^l + i\sqrt{\kappa_l \gamma_s} \eta_{2,3}^l, \quad (30b)$$

where we defined the four new real noises

$$\eta_{1,4}^l = \mathbf{w}_{1,4}^l \cdot \boldsymbol{\xi}_l(t) = \text{Re}\{\xi_l \pm \xi_l^+\}, \quad (31a)$$

$$\eta_{2,3}^l = -i\mathbf{w}_{2,3}^l \cdot \boldsymbol{\xi}_l(t) = \text{Im}\{\xi_l \mp \xi_l^+\}, \quad (31b)$$

which satisfy the statistical properties

$$\langle \eta_j(t) \rangle = 0, \quad \langle \eta_m(t_1) \eta_n(t_2) \rangle = \delta_{mn} \delta(t_1 - t_2). \quad (32)$$

Eqs. (30) are solved with standard methods. The variance spectra for projections  $c_j$ , defined as

$$\tilde{C}_j(\omega) = \int_{-\infty}^{+\infty} d\tau e^{-i\omega\tau} \langle c_j(t), c_j(t+\tau) \rangle. \quad (33)$$

reads, in the stationary limit  $t \gg \lambda_j^{-1}$ ,

$$\tilde{C}_{1,3}^l(\omega) = -\tilde{C}_{2,4}^l(\omega) = \pm \frac{\gamma_s \kappa_l}{[\gamma_s(1 \mp \kappa_l)]^2 + \omega^2}. \quad (34)$$

The advantage of the eigensystem method we are using is that the relevant quadratures of the problem appear in a natural way, as the projections  $c_j^l$  are related to the problem quadratures through

$$X_{c,l} = \sqrt{2} \hat{c}_1^l, \quad X_{s,l} = i\sqrt{2} \hat{c}_2^l, \quad (35a)$$

$$Y_{c,l} = -i\sqrt{2} \hat{c}_4^l, \quad Y_{s,l} = \sqrt{2} \hat{c}_3^l, \quad (35b)$$

where  $(X_{j,l}, Y_{j,l})$  refer to the hybrid mode  $H_{j,(f-l)/2}^l(\mathbf{r})$  as it can be easily seen from (12). These simple relations are the consequence of the appropriate choice of the eigenvectors of  $\mathcal{L}_l$  [15].

We are now in conditions to find out the squeezing spectra of the quadratures. By using Eq. (17) together with the relations above, we get that  $S_{x,c,l}^{out}(\omega) = S_{x,s,l}^{out}(\omega) = 4\gamma_s \tilde{C}_1^l(\omega)$  and  $S_{y,c,l}^{out}(\omega) = S_{y,s,l}^{out}(\omega) = 4\gamma_s \tilde{C}_3^l(\omega)$ , i.e., the squeezing of the phase quadratures are

$$S_{y,j,l}^{out}(\omega) = -\frac{4\kappa_l}{(1 + \kappa_l)^2 + (\omega/\gamma_s)^2}, \quad j = c, s. \quad (36)$$

This expression clearly shows that the phase quadratures of both  $H_{c,(f-l)/2}^l(\mathbf{r})$  and  $H_{s,(f-l)/2}^l(\mathbf{r})$  modes are non-critically squeezed (maximally at  $\omega = 0$ ) for all values of  $l$ , and with different amounts of squeezing depending on the value of the ratio  $\kappa_l$ . This is the main results of our article and we pass to discuss it.

Notice finally that Eq. (36) predicts perfect squeezing at  $\omega = 0$  for  $l = l_0$  as in this case  $\kappa_{l_0} = 1$ . Although the derivation we have presented here has been made for  $l > l_0$ , it is however still valid for  $l = l_0$  with odd  $l_0$  for the hybrid mode that is rotated  $\pi/2$  with respect to the one in which classical emission occurs above threshold (see the discussion of the previous subsection). This result is thus the generalization of our result in ([13]) for  $f > 1$  and odd  $l_0$ .

### C. Discussion

We have shown that the light emitted by a DOPO with a large Fresnel number cavity with spherical mirrors exhibits a variety of squeezing properties. On the

one hand there is the usual critical squeezing appearing at the oscillation threshold [2]. There is also the non-critical squeezing due to the spontaneous breaking of the rotational symmetry that appears above threshold when  $l_0 = 1$  [13]. The new result that we have derived is that also all Hybrid modes with  $l > l_0$ , which remain off at the classical level once the oscillation threshold is crossed, are non-critically squeezed, as shown by Eq. (36).

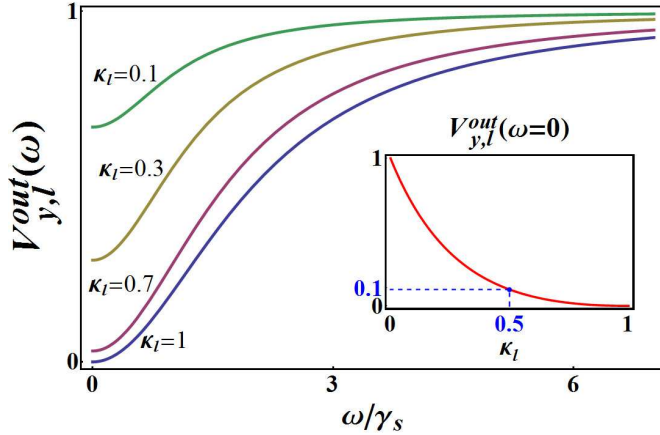


Fig. 3.- Variance spectra of the phase quadratures of some Hybrid modes with  $l \neq l_0$ . The inset shows the same quantity at  $\omega = 0$  as a function of  $\kappa_l$ .

The variance spectrum for either of the phase quadratures  $V_{y,l}^{out}(\omega) = 1 + S_{y,j,l}^{out}(\omega)$  for  $j = c$  or  $j = s$ , is represented in Fig. 3 for different values of  $\kappa_l$ , see Eq. (22). In the figure,  $V_{y,l}^{out}(\omega = 0)$  is also shown, at the inset, as a function of  $\kappa_l$ . Clearly, as  $\kappa_l = \chi_l/\chi_{l_0} \rightarrow 1$ , what occurs as  $l \rightarrow l_0$ , nearly perfect squeezing is found at  $\omega = 0$ . Notice that more than 90% of squeezing can be achieved if  $\kappa_l > 0.5$ . But the ratio  $\kappa_l = \chi_l/\chi_{l_0}$ , which is obtained from Eq. (14), is solely determined by geometrical reasons, and thus the squeezing properties of these higher OAM modes do not depend on the system parameters (of course we must remind that we assumed equal cavity losses for all modes).

In order to better appreciate the large amounts of squeezing exhibited by these modes, we give their associated noise reduction in percentage for different even (odd) families in Table 1 (2). Notice that the largest squeezing occurs for large values of  $f$  and small values of  $l$ , and works better for even families.

Table 1						
$f \setminus l$	2	4	6	8	10	12
2	88.9					
4	96.0	49.0				
6	98.0	71.0	18.1			
8	98.8	81.6	36.8	5.6		
10	99.2	87.4	51.4	14.7	1.6	
12	99.4	90.9	62.1	24.9	5.1	0.4

Table 2						
$f \setminus l$	3	5	7	9	11	13
3	75.0					
5	88.9	33.1				
7	93.8	55.6	10.8			
9	96.0	69.1	24.9	3.1		
11	97.2	77.6	38.0	9.1	0.9	
13	98.0	83.0	49.0	16.6	3.0	0.2

Fig. 4.- Percentage of noise reduction for the non amplified Hybrid modes  $l \neq l_0$  laying in even (Table 1) or odd (Table 2) families. Note that large levels of squeezing are obtained for the lower angular momentum modes.

It is to be remarked that both  $H_{s,p}^l(\mathbf{r})$  and its orthogonal  $H_{s,p}^l(\mathbf{r})$  have the same squeezing properties. This means that the orientation of the mode is irrelevant, as an hybrid mode rotated an arbitrary angle  $\beta$  respect to the  $x$  axis, which is given by

$$H_{\beta,p}^l(\mathbf{r}) = H_{c,p}^l(r, \phi - \beta) = H_{c,p}^l(\mathbf{r}) \cos l\beta + H_{s,p}^l(\mathbf{r}) \sin l\beta, \quad (37)$$

also has the same squeezing properties. This is in clear contrast to the perfectly squeezed mode in the  $l = 1$  case [13] which has not an arbitrary orientation but is orthogonal to the classically excited mode at every instant. Of course, the reason is that the modes here analyzed are below their threshold, at difference with the case in [13].

So far we have proven that the higher OAM modes show noise reduction in their phase quadrature. Let us see why is this occurring. The coefficient that rules the squeezing properties of the  $l \neq l_0$  modes is  $\kappa_l$ , see Eq. (36). Both above and below threshold,  $\kappa_l$  can be written in terms of the stationary pump field as  $\kappa_l = \chi_l \bar{\alpha}_{00}/\gamma_s$ . Below threshold  $\bar{\alpha}_{00}$  increases linearly with the external pump amplitude, see Eq. (20), and hence so does  $\kappa_l$ . But once the bifurcation is reached and the DOPO starts emitting the  $l_0$  mode(s), the value of  $\bar{\alpha}_{00}$  saturates, and remains constant irrespective of the pump value, see Eq. (21). This implies that the value of  $\kappa_l$  will remain fixed to that at the bifurcation once the DOPO is above threshold and consequently, the squeezing level of these modes becomes non-critical.



## VI. CONCLUSIONS

We have shown that tuning large Fresnel number DOPOs, with spherical mirrors, to transverse families is a simple way for generating squeezed light with the shape of Hybrid Laguerre–Gauss modes with OAM  $l > l_0$ , being  $l_0 = 0$  or 1 depending on the even or odd character of the selected family. The behaviour of the system can be resumed as follows: Above threshold, only the mode with  $l = l_0$  is amplified, and the rest of modes (those with  $l > l_0$ ) remain off. The amplified modes exhibit squeezing properties that can be found in the literature (see [2] for  $l_0 = 0$  and [13] for  $l_0 = 1$ ).

The surprising result is that Hybrid modes with  $l > l_0$  exhibit a large degree of squeezing together with the fact that this squeezing is non-critical, i.e., it remains fixed irrespective of the pump value when the system is above threshold. Thus, squeezed vacua with the shape of higher order Hybrid modes are generated by normal DOPOs if these have a large Fresnel number.

In our model we assumed equal cavity losses for all signal modes (this is the precise meaning we give to the expression large Fresnel number cavity) and perfect cavity resonance for a particular family of modes. We do not expect that detuning changes qualitatively this result, as detuning affects equally all modes within the same family (apart, of course, from the fact that there will be particular values of the detuning for which competition phenomena between different families will manifest). Differences in the values of the decay rates for the different modes within the same family could also modify quantitatively the results we have presented, as this would change the threshold for the different modes, a fact that is important in our derivation. In fact, by tailoring the cavity losses for the different modes, one could obtain even smaller quantum fluctuations for these empty modes if their corresponding thresholds are made closer to that of the  $l_0$  mode.

We finally note that Laguerre–Gauss modes are becoming important for several purposes, e.g. in quantum information processing and in manipulation of atoms [8] just to mention a couple. We hope that our results could be of relevance as squeezed Hybrid modes or, equivalently, entangled Laguerre–Gauss modes could be of utility for these purposes.

This work has been supported by the Spanish Ministerio de Educación y Ciencia and the European Union FEDER through Project FIS2005-07931-C03-01. One of us, C. N.-B. is a grant holder of the FPU programme of the Ministerio de Educación y Ciencia (Spain).

## VII. APPENDIX I

Next we outline the derivation of the Langevin Eqs. (15). Neglecting the effect of thermal photons, the master equation ruling the evolution of the system's density

operator [17] reads

$$\frac{\partial}{\partial t} \hat{\rho} = \sum_l \frac{\chi_l}{1 + \delta_{0l}} \left[ \hat{a}_{00} \hat{a}_{+l}^\dagger \hat{a}_{-l}^\dagger - \hat{a}_{00}^\dagger \hat{a}_{+l} \hat{a}_{-l}, \hat{\rho} \right] + \mathcal{E} \left[ \hat{a}_{00}^\dagger - \hat{a}_{00}, \hat{\rho} \right] + \sum_{m=00, \pm l} \gamma_m (2 \hat{a}_m \hat{\rho} \hat{a}_m^\dagger - \hat{a}_m^\dagger \hat{a}_m \hat{\rho} - \hat{\rho} \hat{a}_m^\dagger \hat{a}_m) \quad (38)$$

where losses are assumed to occur in only one of the cavity mirrors. Now we use the positive  $P$ -representation [16, 18] of the density operator, which allows the evaluation of expected values of normally ordered operators as averages of functions in phase space. By using standard methods [16, 18], the master equation (38) is then transformed into a Fokker-Planck type equation for  $P(\boldsymbol{\alpha}, \boldsymbol{\alpha}^+)$ . This equation reads

$$\frac{\partial}{\partial t} P = \left[ - \sum_i \frac{\partial}{\partial \alpha_i} A_i + \frac{1}{2} \sum_{i,j} \frac{\partial^2}{\partial \alpha_i \partial \alpha_j} \mathcal{D}_{ij} \right] P, \quad (39)$$

with

$$A_1 = \mathcal{E} - \gamma_p \alpha_{00} - \sum_l \frac{\chi_l}{1 + \delta_{0l}} \alpha_{-l} \alpha_{+l}, \quad (40)$$

$$A_{3,5} = -\gamma_s \alpha_{\pm l} + \chi_l \alpha_{00} \alpha_{\pm l}^+, \quad (41)$$

$$\mathcal{D}_{35} = \mathcal{D}_{53} = \chi_l \alpha_{00}, \quad \mathcal{D}_{46} = \mathcal{D}_{64} = \chi_l \alpha_{00}^+, \quad (42)$$

and  $A_2$  is obtained from  $A_1$  (as well as  $A_{4,6}$  are obtained from  $A_{3,5}$ ) by changing  $\alpha_j$  by  $\alpha_j^+$  and viceversa. Any other element of the diffusion matrix  $\mathcal{D}$  is null. We have changed the notation so that all the coherent amplitudes are collected into the vector

$$\boldsymbol{\alpha} = \text{col}(\alpha_{00}, \alpha_{00}^+, \alpha_{+l}, \alpha_{+l}^+, \alpha_{-l}, \alpha_{-l}^+). \quad (43)$$

Next, as stated by the Itô theorem [21], this Fokker-Planck equation is mapped onto the set of coupled stochastic (Langevin) equations

$$\dot{\boldsymbol{\alpha}} = \mathbf{A}(\boldsymbol{\alpha}) + \mathbf{B}(\boldsymbol{\alpha}) \cdot \boldsymbol{\eta}(t), \quad (44)$$

where  $\boldsymbol{\eta}$  is a vector with real white noises as components, each of them satisfying the statistical properties defined in (32);  $\mathbf{A}$  is a vector with components  $A_i$ ,  $i = 1, 6$ , defined above; and the *noise matrix*  $\mathbf{B}$  is defined by  $\mathcal{D} = \mathbf{B} \cdot \mathbf{B}^T$ . The equivalence between the Fokker-Planck equation and the Langevin system has to be understood as  $\langle f(\boldsymbol{\alpha}) \rangle_P = \langle f(\boldsymbol{\alpha}) \rangle_{\text{stochastic}}$ , i.e., phase space averages are equal to averages made by using the statistical properties of the noise vector  $\boldsymbol{\eta}(t)$ .

As for the diffusion matrix  $\mathcal{D}$ , it is composed of uncoupled minors for each one of the  $\pm l$  and 00 subspaces, and then so does matrix  $\mathbf{B}$ . In addition, the noise matrix minor associated to the pump mode is the zero matrix as this is its associated minor in  $\mathcal{D}$ . One possible choice for the minors associated to  $\pm l$  modes is

$$\mathbf{B}_l = \sqrt{\frac{\chi_l}{2}} \begin{pmatrix} \sqrt{\alpha_{00}} & 0 & i\sqrt{\alpha_{00}} & 0 \\ 0 & \sqrt{\alpha_{00}^+} & 0 & i\sqrt{\alpha_{00}^+} \\ \sqrt{\alpha_{00}} & 0 & -i\sqrt{\alpha_{00}} & 0 \\ 0 & \sqrt{\alpha_{00}^+} & 0 & -i\sqrt{\alpha_{00}^+} \end{pmatrix}, \quad (45)$$



for  $l \neq 0$  and

$$\mathcal{B}_0 = \sqrt{\chi_0} \begin{pmatrix} \sqrt{\alpha_{00}} & 0 \\ 0 & \sqrt{\alpha_{00}^+} \end{pmatrix}, \quad (46)$$

for  $l = 0$ . Finally, inserting this noise matrix into the equivalent Langevin system (44), we get the Eqs. (15).

- 
- [1] R. Loudon and P. L. Knight, J. Mod. Opt. **34**, 709 (1987)
- [2] D.F. Walls and G.J. Milburn, *Quantum Optics* (Springer, Berlin, 1994).
- [3] P. D. Drummond and Z. Ficek (eds.), *Quantum Squeezing* (Springer Verlag, Berlin, 2004).
- [4] J. Gea-Banacloche, N. Lu, L.M. Pedrotti, S. Prasad, M.O. Scully, and K. Wódkiewicz, Phys. Rev. A **41**, 369 (1990).
- [5] H. Vahlbruch et al., Phys. Rev. Lett. **100**, 033602 (2008); see also Y. Takeno et al., Opt. Express **15**, 4321 (2007).
- [6] S.L. Braunstein and P. van Loock, Rev. Mod. Phys. **77**, 513 (2005).
- [7] C. Fabre et al., Opt. Lett. **25**, 76 (2000); N. Treps et al., Phys. Rev. Lett. **88**, 203601 (2002); N. Treps et al., Science **301**, 940 (2003).
- [8] See, e.g., S. Franke-Arnold and A.S. Arnold, American Scientist **96**, 226 (2008).
- [9] A. Gatti, L.A. Lugiato, Phys. Rev. A **52**, 1675 (1995).
- [10] I. Pérez-Arjona, E. Roldán, and G.J. de Valcárcel, Europhys. Lett. **74**, 247 (2006).
- [11] I. Pérez-Arjona, E. Roldán, and G.J. de Valcárcel, Phys. Rev. A **75**, 063802 (2006).
- [12] K.I. Petsas, A. Gatti and L.A. Lugiato, Quantum Semi-class. Opt. **10**, 789 (1998).
- [13] C. Navarrete-Benlloch, E. Roldán, and G.J. de Valcárcel, Phys. Rev. Lett. **100**, 203601 (2008).
- [14] N. Hodgson and H. Weber, *Laser resonators and beam propagation* (Springer, New York, 2005).
- [15] It is worth remarking one point on the diagonalization of operator  $\mathcal{L}_l$ . Its eigensystem consists of two degenerate subspaces. How must the two eigenvectors expanding each degenerate subspace be chosen? As will become clearer later, the more appropriate choice is the one that make the operators related to the projections  $c_j$  be either Hermitian or anti-Hermitian, so that they coincide (up to a real or imaginary constant) with some observable of interest. For example, with our choice of eigenvectors we see that the operators related to  $c_1^l$  and  $c_2^l$  are  $\hat{c}_{1,2}^l = \hat{a}_{+l} \pm \hat{a}_{+l}^\dagger \pm \hat{a}_{-l} + \hat{a}_{-l}^\dagger$ , see (29), which are Hermitian and anti-Hermitian, respectively.
- [16] P.D. Drummond and C.W. Gardiner, J. Phys. A: Math. Gen. **13**, 2353 (1980).
- [17] H.J. Carmichael, *Statistical Methods in Quantum Optics 1* (1999, Springer, Berlin).
- [18] C. W. Gardiner and P. Zoller, *Quantum Noise* (Springer, 2000).
- [19] M.J. Collet and C.W. Gardiner, Phys. Rev. A **30**, 1386 (1984).
- [20] A. Gilchrist, C.W. Gardiner, and P.D. Drummond, Phys. Rev. A **55**, 3014 (1997).
- [21] L. Arnold, *Stochastic differential equations: theory and applications* (John Wiley and sons, New York, 1974).